IJREAT International Journal of Research in Engineering & Advanced Technology, Volume 3, Issue 1, Feb-Mar, 2015
ISSN: 2320 – 8791 (Impact Factor: 1.479)
www.ijreat.org

Effect on Wind Pressures by Variation of Roof Pitch of Low-Rise Hip-Roof Building

H. Irtaza[1], M. A. Javed[2], A. Jameel[3]

[1]Associate Professor, Dept. of Civil Engineering, A.M.U., Aligarh, U.P., 202002, India

[2]Research Assistant, Dept. of Civil Engineering, A.M.U., Aligarh, U.P., 202002, India

[3]Associate Professor, University Polytechnic, A.M.U., Aligarh, U.P., 202002, India

Abstract

The paper presents a numerical study of wind pressure on the low-rise hip-roof building by varying the roof pitch using computational fluid dynamics (CFD). A Texas Tech. University building models with hip roof, reduced at a geometric scale of 1:50 were numerically simulated for the present study. Various hip-roof building models of different roof pitches as usually used in different parts of the world, such as, 15°, 20°, 30° and 40° were selected with different wind angle attack i.e. 0°, 45° and 90°. The numerically computed wind pressure coefficients on the roof of the hip-roof buildings were compared with the wind-tunnel results. Two RANS (Reynolds Averaged Navier-Stokes) turbulence models such as the Standard $k-\varepsilon$ (SKE) and the Renormalization group $k-\varepsilon$ (RNG-KE) were adopted in this study keeping in mind the computational resources available.

Result shows that roof pitch does affect the magnitude of wind pressures coefficients but the pattern almost remains same. The model with roof pitch 30° amongst the various models was found to have maximum wind pressure. It was also found that the results obtained using the CFD turbulence models and the wind-tunnel data are in good agreement with in certain limit.

***Keywords**: Computational Fluid Dynamics, Wind force, Hip-roof building, Low-rise building, RNG, SKE, Wind Engineering.*

1. Introduction

Building with a mean roof height less than about 20 m are categorized as low-rise. Majority of buildings the world over, whether residential or commercial, are low-rise. The effect of varying geometric configurations, surrounding topography and wind directions, etc. make analyses of wind load on low-rise buildings a bit complicated. Dynamic modeling of wind loads on low-rise buildings remains a very challenging task, which is critical for cost-effective design and reduction of wind-induced losses [1].

In different types of terrain and topography, buildings with various plan forms are constructed. The geometry and shape of the building and its roof specifically, influences the wind pressure coming on the particular building. Sharp edges and corners in the buildings show sudden variation in wind pressure distribution and magnitude as well.

In hip-roof building as shown in figure 1 the roof from all sides slope downwards, usually with a fairly gentle slope, to the walls. Thus, it is a house with no gables or other vertical sides to the roof. The geometry of a hip-roof building is such that it bears corners and sharp edges, therefore it is important to study wind load and its effects on a hip-roof building.

A post disaster investigation on wind-induced damage to building roofs was performed by Federal Emergency Management Agency [FEMA]. It was concluded that during severe cyclones, hip roofs perform better than gable roofs [2]. Many researchers have studied the effect of wind forces on low rise buildings including gable and hip-roof. Davenport *et al*. [3] performed a comprehensive wind-tunnel studies on the low rise gable roof buildings concluded that the roof slope affects the wind pressures.

With the aim of predicting the risk of structural damage associated with roof shapes, Sparks *et al*. [4] measured mean wind pressures on both gable and hip-roof in a wind-tunnel. Meecham *et al*. [5] also carried out a comparative study of the magnitude and distribution pattern of wind pressure between a gable roof and a hip-roof. They found that the worst peak pressure on the hip-roof was reduced by as much as 50% from that on the gable roof. In order to study the effect of variation of pitch, Xu *et al*. [6] carried

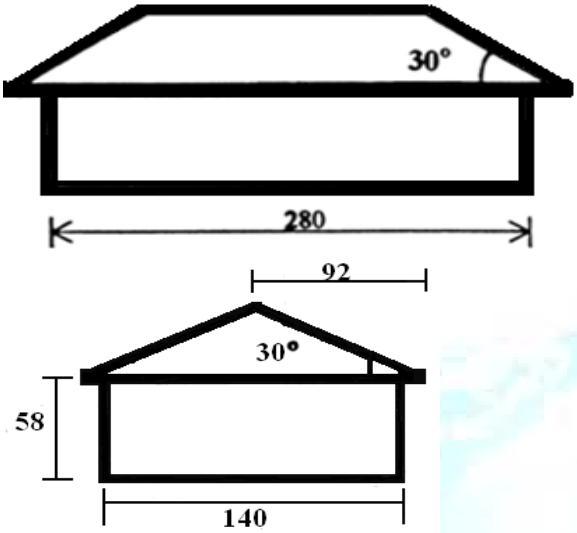

Fig. 1 A typical hip roof building (front and side elevation).

out wind tunnel tests on three hip roof building models of 15°, 20° and 30° roof pitch. The results revealed that the 30° hip roof experiences the highest peak suctions at the corners and the worst peak suctions are much smaller on the hip roofs than on the gable roofs for 15° and 20° roof pitch.

Shakeel *et al* [7] tested a Texas Tech University building model with hip-roof at a reduced geometric scale of 1:50 in atmospheric boundary layer wind-tunnel. They studied the effect of wind pressures on hip-roof building by varying its geometry. The variations were done on the overhang ratio such as 0.17, 0.26, 0.38 and on height ratio such as 0.4, 0.5, 0.6 of the hip-roof building. They found that, both the overhang and aspect ratio influenced the magnitude and distribution pattern of pressures on hip roof. The model with overhang ratio 0.26 amongst the first three models and the model with height aspect ratio 0.6 amongst the next three models have been found to experience maximum peak pressure.

It can be concluded from the studies of the various researchers on low-rise building that the type of roof geometry and the dimension affects the wind load coming on it. The direction of the wind attack on the roof also affects the wind pressure on roofs. All these studies are based on the wind-tunnel tests in the laboratories.

Although, the wind-tunnel tests are being made more effective and reliable, but there are certain limitations associated with it. It is not easily possible to place the pressure taps on the overhang portions, in corner regions, and on sharp edges of the hip-roof building model. The pressure coefficients on these regions are either extrapolated or interpolated from the adjoining data. This problem can be resolved using CFD techniques. So, in the present study, CFD techniques were used to analyze wind pressure on the hip-roof building with roof pitch of 15°, 20° and 30° have been taken in order to study the effect of wind pressure on the roof, with same model dimensions of Shakeel *et al* [7].

2. Numerical Methods

The atmospheric boundary layer (ABL) flow is highly turbulent flow which can be described by the well-known Navier-Stokes equations. Various CFD methods have been widely used in the field of wind engineering over the last two decades. The most common method for the computation of turbulent flows is the Reynolds Averaged Navier-Stokes (RANS) approach, where the equations are averaged in time over all the turbulence scales to directly yield the statistically steady solution of the flow variables. The Spalart-Allmaras, Standard $k-\varepsilon$, RNG $k-\varepsilon$, Realizable $k-\varepsilon$, Standard k-ω, SST k-ω, V2F Model, Reynolds-Stress Model are the models available in Fluent. The choice of turbulence model will depend on considerations such as the physics encompassed in the flow, the established practice for a specific class of problem, the level of accuracy required, the available computational resources, and the amount of time available for the simulation[8].

Other approach is called Large Eddy Simulation (LES) where the small scales of the flow are removed from the flow variables by spatially filtering the Navier-Stokes equations, the influence of the small scales appears at least as sub-filter stresses in the momentum equation and as boundary terms and, if the filter width is not constant, then additional sub-filters arise [9] which have to be modeled in terms of the computed large scale quantities.

The difficulties in applying CFD to wind engineering problems are mainly caused by the following factors [10]: large Reynolds number, impinging at the front, sharp edges of bluff bodies, remaining effects of flow obstacle at outflow boundary, etc. Therefore, several revisions of turbulence models have been made to overcome these difficulties. For the turbulence models used in RANS, two different approaches are used. The first approach is based on the eddy viscosity assumption and models the turbulent

stresses by analogy to the molecular stresses derivatives of the mean velocity. Of these models, the standard $k-\varepsilon$ model has the drawback of not being able to predictthe wind conditions in the separation regions above roof surfaces and near side walls of bluff bodies [11], due principally to the overproduction of turbulent kinetic energy in regions of stagnant flow. Several ad-hoc modifications of the model have been proposed [12] but their better prediction of pressure coefficients in front of buildings led to worse predictions of the velocities, especially in the wake of obstacles [13, 14]. More advanced revised $k-\varepsilon$ models like the Renormalizationgroup (RNG) $k-\varepsilon$model of Yakhot et al [15] or the realizable $k-\varepsilon$model of Shih et al [16] have attracted more interest because they attenuate the stagnation point anomaly without leading to worse results in the wake.

A general view on numerical simulation of wind engineering problems is that the standard turbulence models used in most codes (eddy viscosity based models or the various second-order stress models) are inadequate in many respects, in particular to study flow around bluff bodies, and that a time-dependent approach can yield more accurate results than statistically steady RANS simulations. LES is in principle the most general method to lead to better results in the prediction of bluff body flows and it becomes imperative for proper identification of the important unsteady features of such flows, which are very useful for investigating wind-induced vibrations of buildings and structures. This is however obtained at a significant higher cost in CPU times which are unrealistic for some engineering applications. But the advances of computational resources in recent years are helping LES to attract more attention in wind engineering. Murakami [17] has shown that LES with a dynamic subgrid-scale (SGS) model is a promising tool for accurately predicting the flow field around a bluff body compared with other turbulence models, with dynamic models leading to improved results for the flow around a square cylinder in comparison to the constant viscosity Smagorinsky model [17]. Rodi [18] compared LES and RANS predictions of a cube-in-a-channel flow to observe that LES can basically capture all the complex features of the cube flow fairly well, even quantitatively. However, there are still some limits for LES to be applied effectively in solving practical problems in wind engineering. The first limit has been already mentioned, LES also needs models for the filtered small scales. Additionally to the classical Smagorinsky model [17], other SGS models have been proposed [19, 20, 21, 22]. To obtain accurate simulation results of wind flows around bluff bodies, especially for cases with high Reynolds number, a suitable *SGS* model should be carefully chosen. The second limit is the near wall treatment. Full solution of near wall turbulence of a bluff body needs very fine grid resolution, especially for separated boundary flows, which often makes full-scale LES inapplicable due to the huge amount of mesh numbers required. The fact that most commercial or open-source codes now include LES modules is bound to make the application of LES even more widespread. In wind engineering, for example, Nozawa and Tamura [23] determined mean and fluctuating surface pressures on a half-cube model, Ono et al [24] made an analysis of conical vortex structures generated on the roof of a flat building at 45º to the approach flow, Huang *et al* [10] used LES and RANS models for the study of wind effects on the Commonwealth Advisory Aeronautical Council standard tall building to explore an effective and reliable approach for evaluation of wind effects on tall buildings by *CFD* techniques, Lim et al [25] studied the flow around a surface mounted cube placed in a turbulent boundary layer tailored to match a series of wind tunnel observations and concluded that, provided properly formulated inflow and surface boundary conditions are used, LES can give the mean and fluctuating surface pressures on isolated bodies with a similar degree of uncertainty as usually associated with wind tunnel modelling.

In the present study, boundary layer turbulent wind flows around a hip-roof building has been simulated using the Standard $k-\varepsilon$ and the RNG $k-\varepsilon$ turbulence models. Different angles of the building to the approach wind flow are evaluated. For a comparison of the better accuracy of results obtained using RANS models such as the standard $k-\varepsilon$ and RNG $k-\varepsilon$ are compared with those of an extensive wind tunnel test conducted.

3. Numerical Model and Boundary Condition

A hip-roof building as shown in Fig. 1 with the model dimensions of 280 mm x 140 mm and 58mm eave height [Prototype 14 m x 7 m x 2.9 m], with varying roof pitch of 15°, 20°, 30° and 40º were selected for numerical study. The wind attack angle on the model is changed from 0° to 90° at an interval of 15°. The position of hip-roof building model at zero degree incidence angle of wind attack was such that one of the long walls, having length equal to 280 mm, is facing the wind flow and the other is at leeward side of the flow. The smaller walls, having length equal to 140 mm, were parallel to the flow of the wind. Wind incidence angle is then gradually changed with difference of 15°. In the model having wind incidence angle 90°,

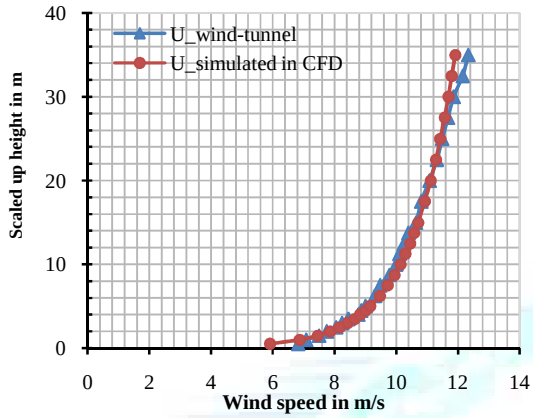

Fig. 2 Profile of wind in wind-tunnel and simulated wind profile for CFD

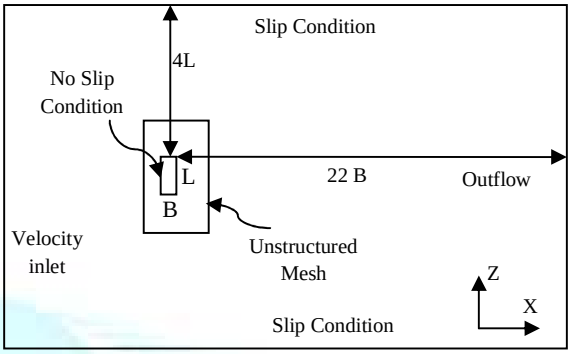

Fig. 3 Computational domain and boundary condition in plan at eave level

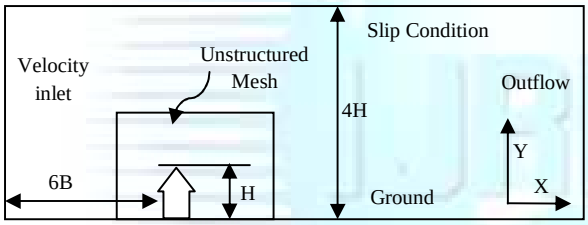

Fig. 4 Computational domain and boundary condition in elevation parallel to the flow of the wind

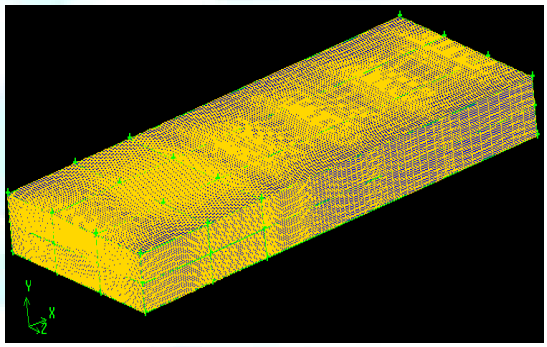

Fig. 5 Mesh arrangement for whole computational domain

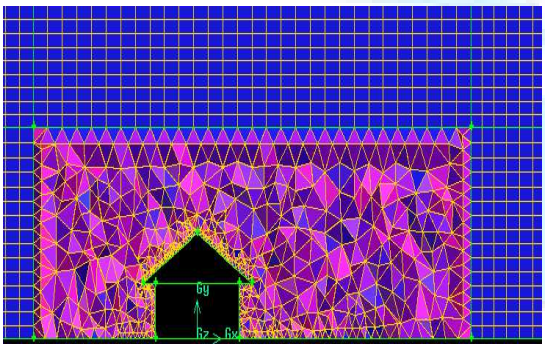

Fig. 6 Mesh arrangement near the building in the plane at mid length of the building, parallel to the flow of the wind

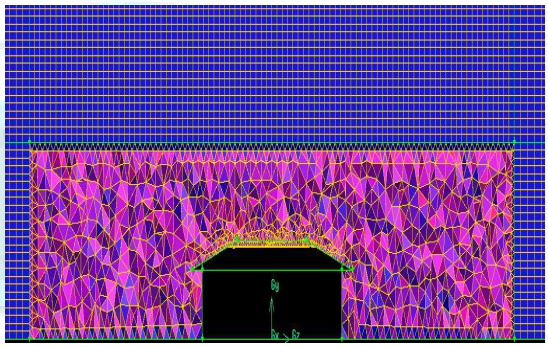

Fig. 7 Mesh arrangement near the building in the plane at mid length of the building, perpendicular to the flow of the wind

wind attack was such that one of the small walls is facing the wind flow and the other one is on the leeward side of the flow. The longer walls in this model were parallel to the flow of the wind.

The difference in boundary conditions may cause large variation in results obtained from wind-tunnel tests and CFD simulation. In order to obtain better agreement between results of both methods, boundary conditions adopted in the numerical simulations should be the same as those in the experiments, especially for inflow boundary conditions. Taking this into consideration, the inlet wind-profile as shown in the Fig. 2 and other wind properties such as turbulence intensity of 18% and integral length scale 0.45 m at eave height were taken from the experimental work of Shakeel *et al* [7]. The mean longitudinal wind speed profile of Shakeel *et al*. measured in the wind-tunnel is in good accordance with full-scale profile with a power-law exponent of 0.15 whereas that of Xu *et al*. the power law exponent is 0.14 (Other parameters taken by Xu *et al*. were turbulence intensity of 20%, integral length scale 0.8 m at eave height [6]). The other parameters such as friction velocity($u_\tau = 0.567 m/s$) and ground roughness length (9-10 mm) were derived from the wind-tunnel data of Shakeel *et al*. The other boundary conditions can be seen in the Figure 3 & 4.

4. Computational Simulation

Gambit 2.6 [26] has been used for the making the models and generation of meshes on and around the model. Fig. 5 shows a hip-roof building inside a computational domain. The computational domain covers 29B (B is overall length of the building model along the wind flow including overhangs) in the stream wise X direction, $[-6.5 < (x/B) < 22.5]$, 9L in the lateral or normal (Z) direction $[-4.5 < (z/B) < 4.5]$ and 4H in the vertical (Y) direction. As explained by Murakami *et al* [27], such a choice for computational domain is required in order to remove the flow obstacles.

The hip roof building is further surrounded in a rectangular box with in the computational domain which is much larger than the hip roof building model (three times in width, four times in length and two times in height). For efficient computation of turbulence, the mesh arrangements should be fine enough near the building surface, that's why the unstructured mesh is applied within the core rectangular box around the hip-roof building model. It is because unstructured meshes can easily be stretched or contracted in particularly in regions of sharp edges. Since large mesh can increase computational cost that's why regions away from the building are meshed with coarser structured mesh, whereas in the regions near the building coarser meshes were provided as can be seen in Fig. 6 & 7. The sharp edges, overhangs and corners within the hip-roof building makes its geometry quite complicated forcing to use unstructured meshes which helps in generating quality meshes within those regions.

The Reynolds numbers involved in the simulations were in the range of 1.25×10^5 to 2.22×10^5 for both wind-tunnel experiments and computational analyses. The percentage obstructions were 1.93 and 2.22when the wind attack angles on the model of the hip-roof building were 90° and 0°respectively for 30° roof pitch. For a better simulation of any model in wind-tunnel test or the CFD simulations on any model of the structure, the maximum obstructions should not be more than 3%. The reason for such choice was to eliminate the flow obstacle effect on the inflow and outflow boundary conditions.

The solver used in the present study is Fluent Inc. 6.2.16. This solver uses the finite-volume method to solve the governing equations and boundary conditions associated with it. A fundamental assumption of using finite-volume method is that the body is divided into small discrete regions known as finite elements. These elements defined by nodes and interpolation functions. Governing equations are written for each element & these elements are assembled into a global matrix. Solutions were done for unsteady-state. Second-order differencing was used for the pressure, momentum and turbulence equations and the "SIMPLE" pressure-velocity coupling approach [8]. The numerical time step for the RNG $k-\varepsilon$ model and the Standard $k-\varepsilon$ model was $2 \times 10^{-3} s$ and in order to obtain the time-averaged results, 4000 steps were iterated. In the present study order of the mesh used is within the range of 10^6 in each model. As standard wall function is used, so the value of y-plus ($y^+ = {\rho u_\tau y}/{\mu}$) is managed within the range of 30 to 150.

5. Result and discussions:

In the present study, the effect of variation of roof pitches on the wind load on hip-roofs has been studied. For this purpose, the wind loads has been obtained on models with four different roof pitches i.e. 15°, 20° 30° and 40°, at three different wind incident angles, i.e. 0°, 45° and 90°. The wind loads have been obtained numerically using CFD techniques and the inflow boundary conditions data

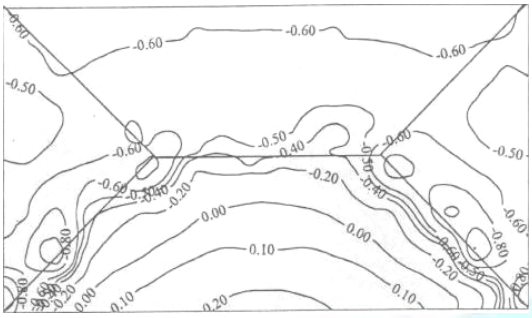

(a) Pressure Coefficients on roof by wind-tunnel experimental data (Shakeel et al)

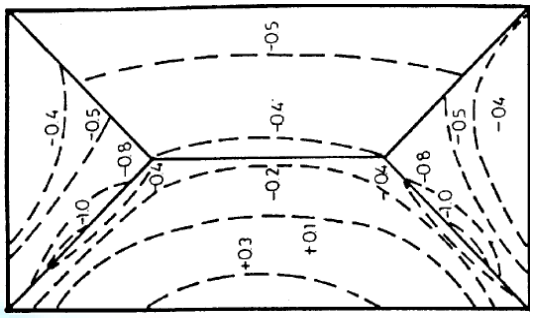

(b) Pressure Coefficients on roof by wind-tunnel experimental data (Xu et al)

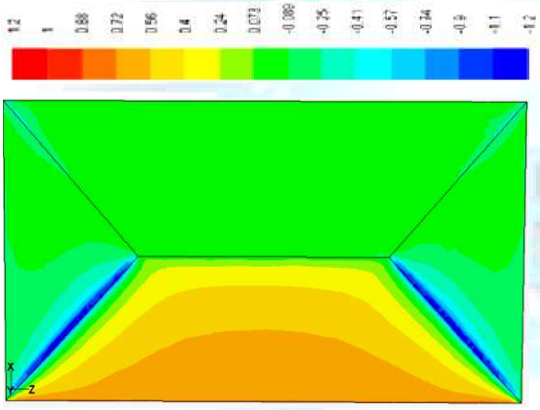

(c) Pressure Coefficients on roof by Std. $k-\varepsilon$ turbulence model

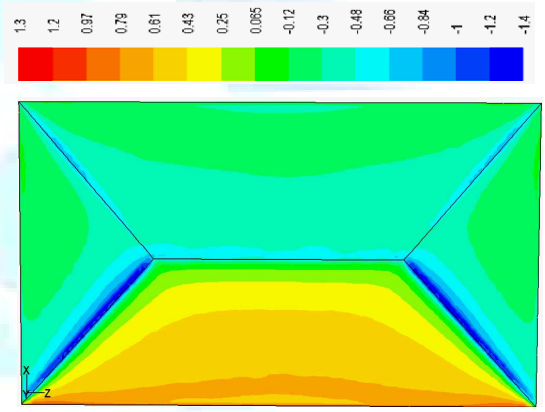

(d) Pressure Coefficients on roof by RNG $k-\varepsilon$ turbulence model

Fig. 8 (a,b,c,d) Comparison of contours plot on the roof of the hip-roof building with 30 degree roof pitch at 0 degree wind attack angle

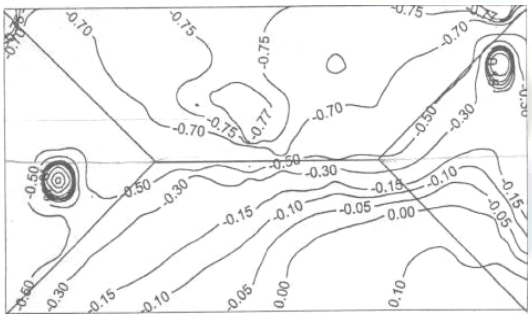

(a) Pressure Coefficients on roof by wind-tunnel experimental data (Shakeel et al)

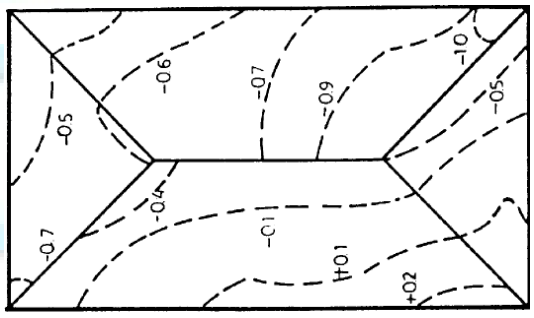

(b) Pressure Coefficients on roof by wind-tunnel experimental data (Xu et al)

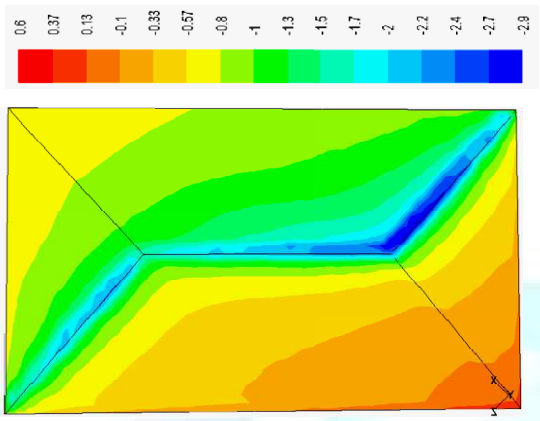

(c) Pressure Coefficients on roof by Std. $k-\varepsilon$ turbulence model

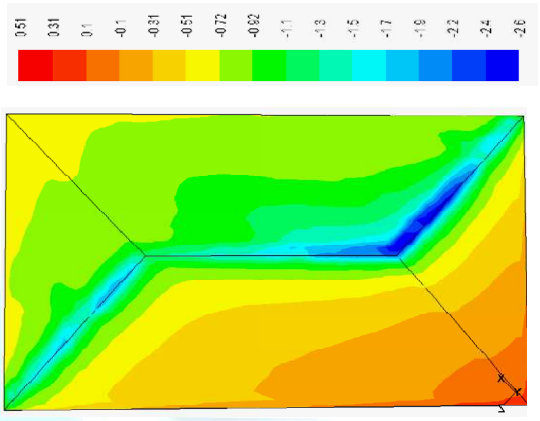

(d) Pressure Coefficients on roof by RNG $k-\varepsilon$ turbulence model

Fig. 9 (a,b,c,d) Comparison of contours plot on the roof of the hip-roof building with 30 degree roof pitch at 45 degree wind attack angle

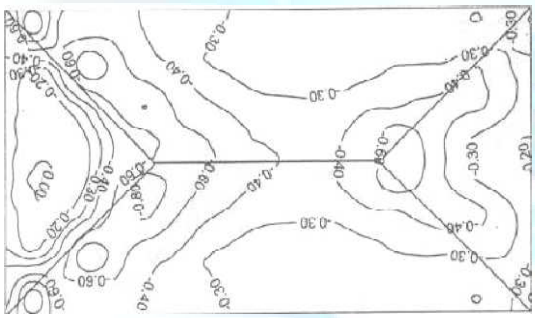

(a) Pressure Coefficients on roof by wind-tunnel experimental data (Shakeel et al)

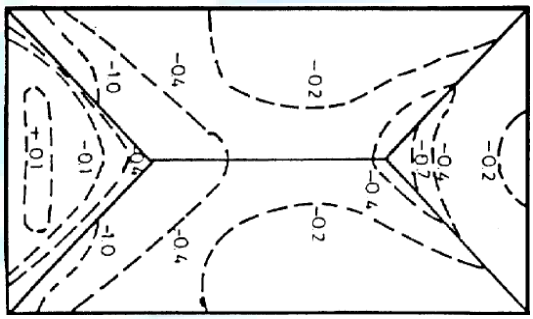

(b) Pressure Coefficients roof by wind-tunnel experimental data (Xu et al)

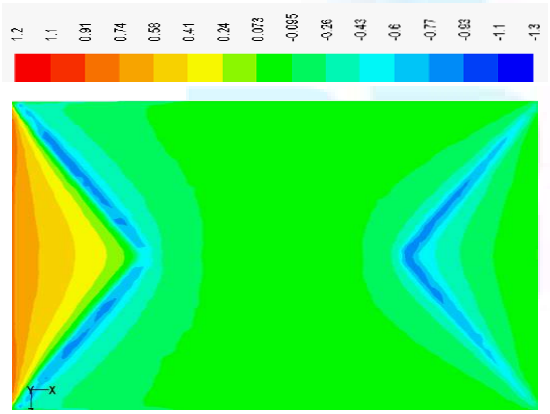

(c) Pressure Coefficients on roof by Std. $k-\varepsilon$ turbulence model

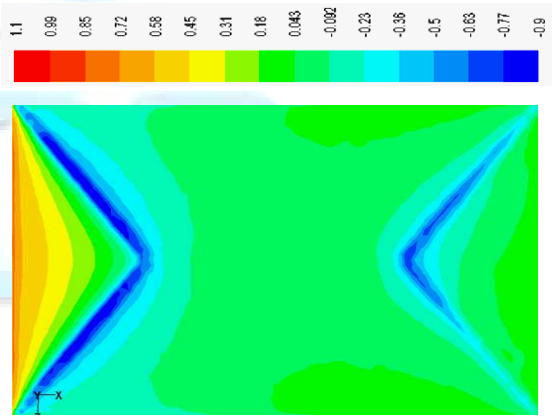

(d) Pressure Coefficients on roof by RNG $k-\varepsilon$ turbulence model

Fig. 10 (a,b,c,d) Comparison of contours plot on the roof of the hip-roof building with 30 degree roof pitch at 90 degree wind attack angle

were taken from the wind tunnel test of Shakeel *et al* for computational simulation. The Reynolds numbers involved in the simulations are more than 10^5, which are in the same range as those encountered in the wind tunnel experiment of Shakeel *et al* [7], In order to get the accurate results grid independent study has been considered and the wall unit is taken within the range of 30-150 for the all cases. The effectiveness of the turbulence models and numerical treatments for solving the practical problem with high Reynolds number were investigated in details. The CFD codes used in this study are Standard and RNG . Fluent Inc. and Gambit softwares have been used to develop model and to mesh the domain.

Fig. 8 to 10 shows the comparison of the wind pressure coefficients obtained from the numerical simulation using the Standard and the RNG turbulence model on the hip-roof with 30° roof pitch to that of the wind-tunnel results on the same models obtained by Shakeel *et al* and Xu *et al* at 0°, 45° and 90° wind incidence angle. For 45° degree wind attack angle, the experimental values of pressure coefficients are less in comparison to CFD simulated values. Whereas for the case of 0° and 90° wind attack angle the wind-tunnel values of pressure coefficients are higher than the CFD simulated values. The maximum pressure coefficient on the roof has been found for 45° wind incidence angle and the least for 90° wind incidence angle. There are certain differences in the results of Shakeel *et al* and Xu *et al* which may be due to difference of wind tunnel. Numerical results obtained in the present study mostly matches with the results of Shakeel *et al*, but in some regions it is more nearer to the results of Xu *et al* also. Overall variation of numerical results from the wind tunnel results is about 10-15%, but near the ridge and near eave level it varies about 30-40%. These discrepancies in the results may be because in wind tunnel models it is difficult to put pressure taps on edge and overhangs and corners. So wind tunnel results are either extrapolated or interpolated for that region.

It has been found that the Standard $k-\varepsilon$ models have a good reputation for its efficiency and easy implementation. Standard $k-\varepsilon$ model can predict the general wind conditions around the building reasonably well, except those in the separated regions above roof surface, due to the overestimation of turbulence energy where the slope of the roof changes. The RNG $k-\varepsilon$ turbulence model was found to be the best choice among the both RANS models for rapid solutions. It gave encouraging results for the mean pressure coefficients in most cases.

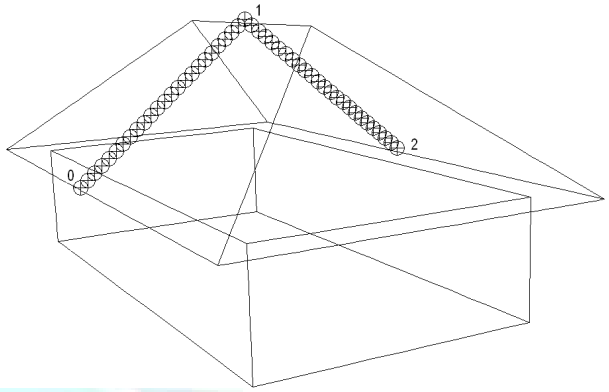

Fig. 11 Pressure Coefficient values are plotted around the rakes shown.

Fig. 12 to 15, shows the wind pressure coefficients obtained from the Standard $k-\varepsilon$ and the RNG $k-\varepsilon$ turbulence models along the rake at mid width on the roof as shown in Fig. 11 at pitch 15°, 20° and 30° were compared with the wind tunnel results obtained from the work of Shakeel et al and Xu et al at a wind incidence angle of 0°, 45° and 90°. It has been found that numerical results and experimental results are in good agreement with each other. Among various wind attack angles, pressure obtained at 90 degree attack angle are more near to the wind tunnel results than that of zero and 45 degree attack angle. Little difference in the pattern is shown by graph of CFD simulation and Shakeel *et al* at zero degree wind attack. Pattern of the plot in 20 degree, 30 degree and 40 degree roof pitch also remains same as that of 15 degree roof pitch. The results obtained by RNGKE are more near to the wind-tunnel results than the Standard KE. In the present graph, overall variation of CFD results from the wind tunnel results is about 10-15%, but near the ridge and near eave level it varies about 35-40%.

Table 1: Maximum values of pressure coefficients

Roof pitch / ***Incident angles***	**15°**	**20°**	**30°**	**40°**
0°	-1.57	-1.45	-1.4	-1.13
45°	-1.34	-2.21	-2.6	-1.53
90°	-0.477	-0.565	-0.77	-1.12

From figure 16 to 18, the comparison of values obtained on different roof pitches has been done. In all the wind attack angles the pattern of graph remains same for both

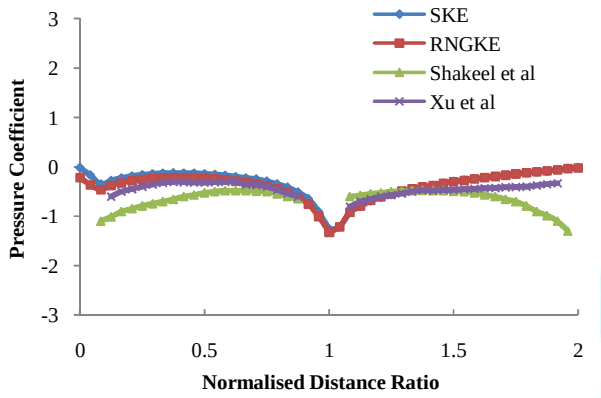

(a) Pressure Coefficients on roof at zero degree wind attack angle

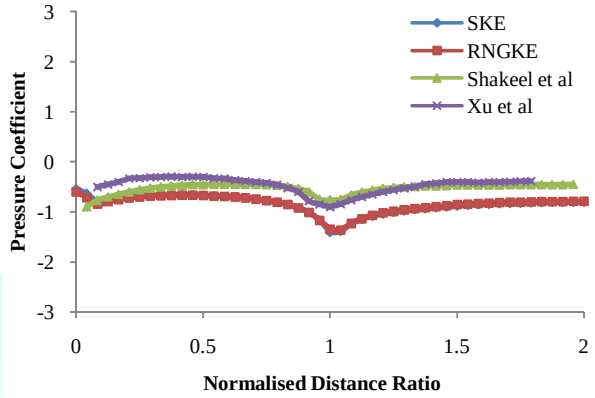

(b) Pressure Coefficients on roof at 45 degree wind attack angle

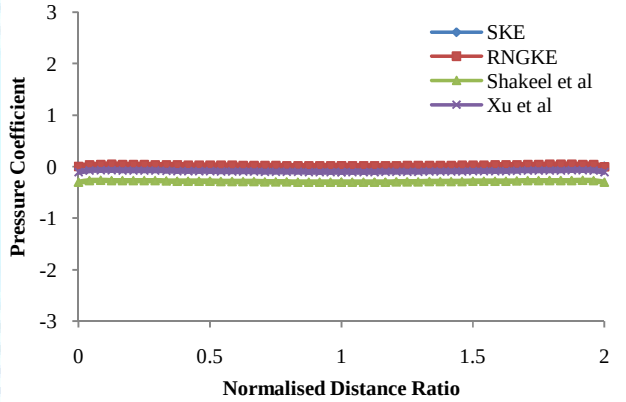

(c) Pressure Coefficients on roof at zero 90 degree attack angle

Fig. 12 (a,b,c) Pressure coefficients on the roof of 15° pitch at different wind incidence angles

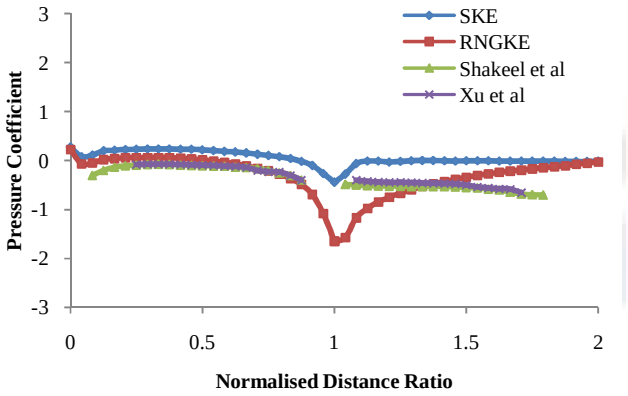

(a) Pressure Coefficients on roof at zero degree wind attack angle

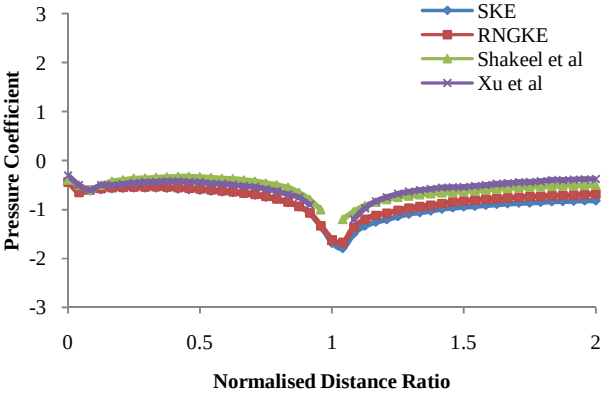

(b) Pressure Coefficients on roof at 45 degree wind attack angle

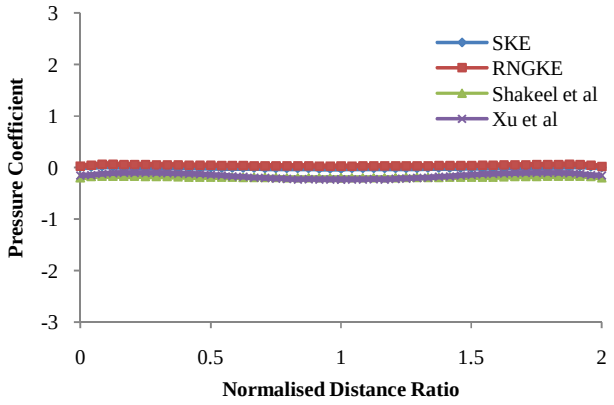

(c) Pressure Coefficients on roof at 90 degree wind attack angle

Fig. 13 (a,b,c) Pressure coefficients on the roof of 20° pitch at different wind incidence angles

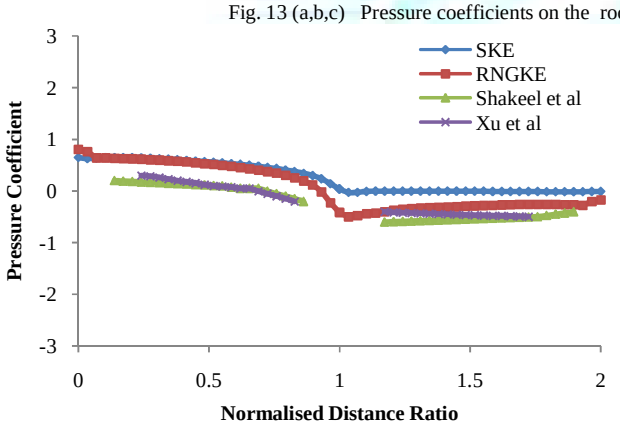

(a) Pressure Coefficients on roof at zero degree wind attack angle

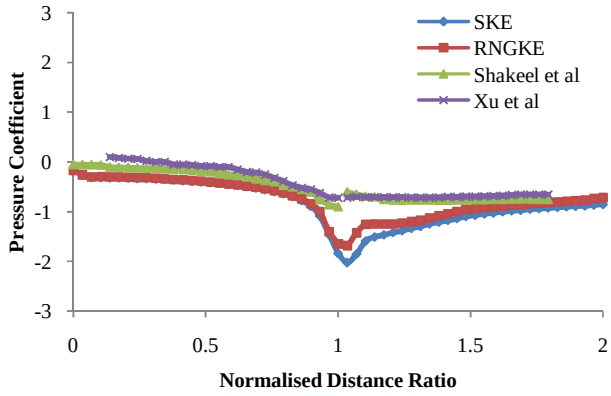

(b) Pressure Coefficients on roof at 45 degree wind attack angle

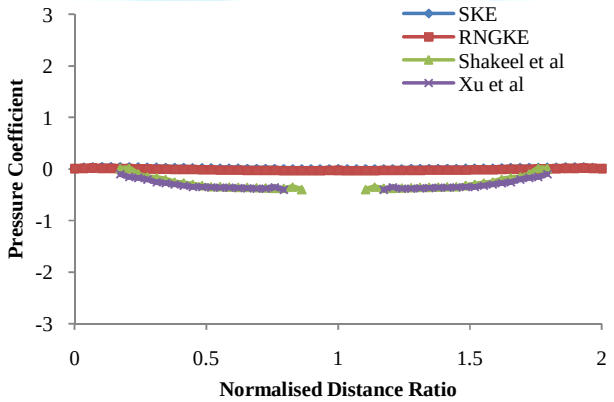

(c) Pressure Coefficients on roof at 90 degree wind attack angle

Fig. 14 (a,b,c) Pressure coefficients on the roof of 30° pitch at different wind incidence angles

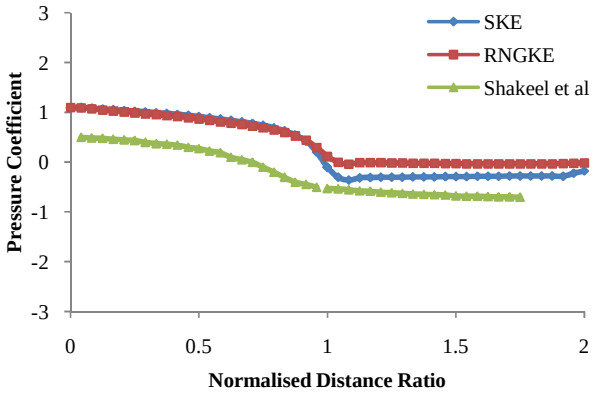

(a) Pressure Coefficients on roof at zero degree wind attack angle

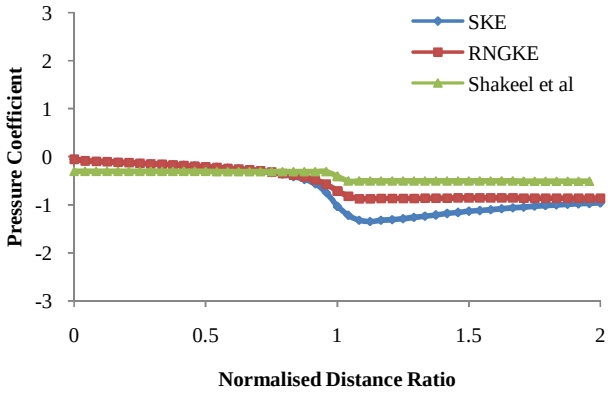

(b) Pressure Coefficients on roof at 45 degree wind attack angle

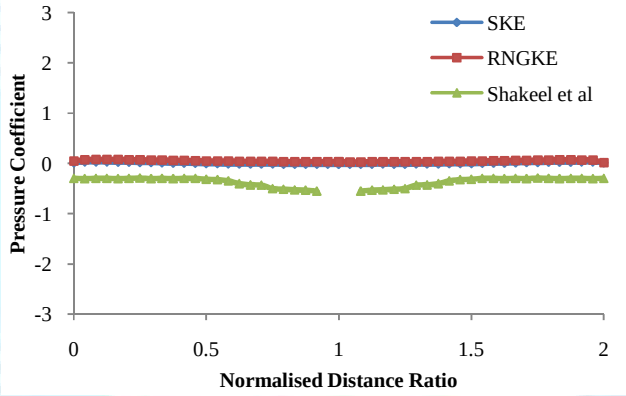

(c) Pressure Coefficients on roof at 90 degree wind attack angle

Fig. 15 (a,b,c) Pressure coefficients on the roof of 40° pitch at different wind incidence angles

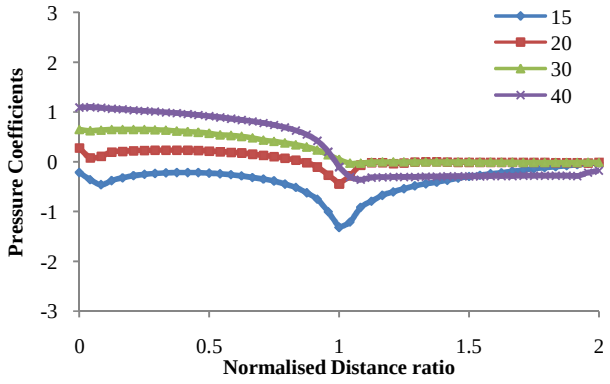

(a) Pressure Coefficients on roof for SKE model

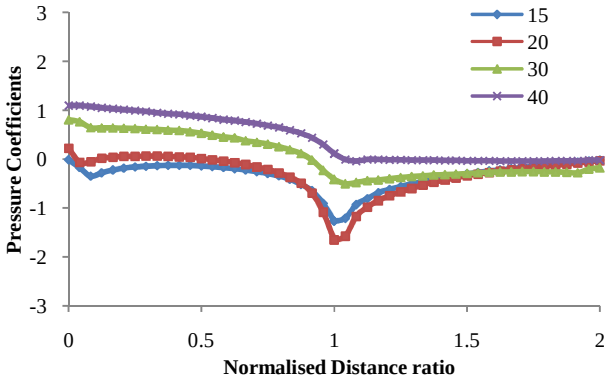

(b) Pressure Coefficients on roof for RNGKE model

Fig. 16 (a,b) Pressure coefficients on the roof at zero degree wind incidence angles for different roof pitches

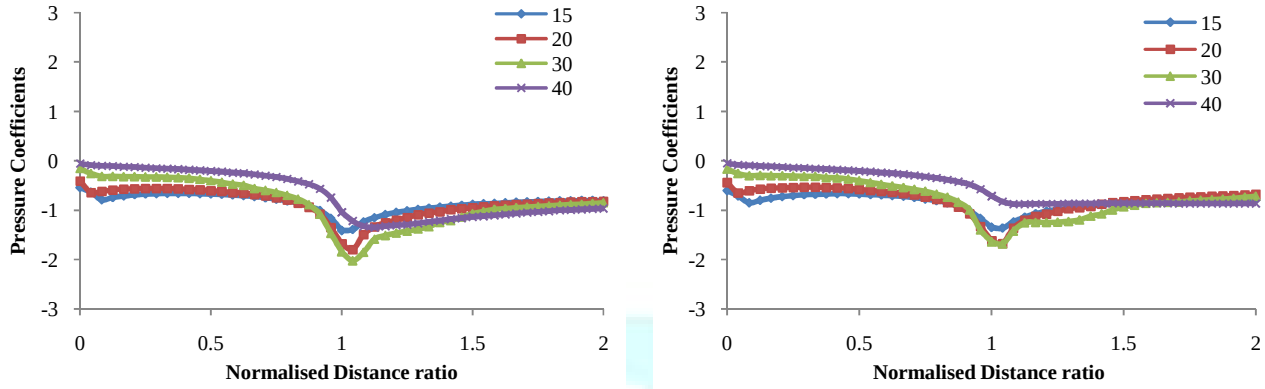

(a) Pressure Coefficients on roof for SKE model (b) Pressure Coefficients on roof for RNGKE model

Fig. 17 (a,b) Pressure coefficients on the roof at 45 degree wind incidence angles for different roof pitches

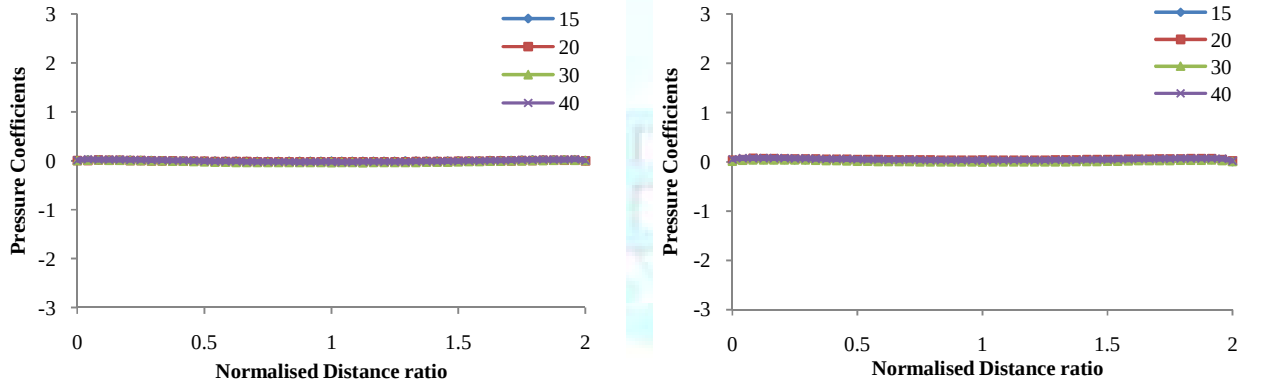

(a) Pressure Coefficients on roof for SKE model (b) Pressure Coefficients on roof for RNGKE model

Fig. 18 (a,b) Pressure coefficients on the roof at 90 degree wind incidence angles for different roof pitches

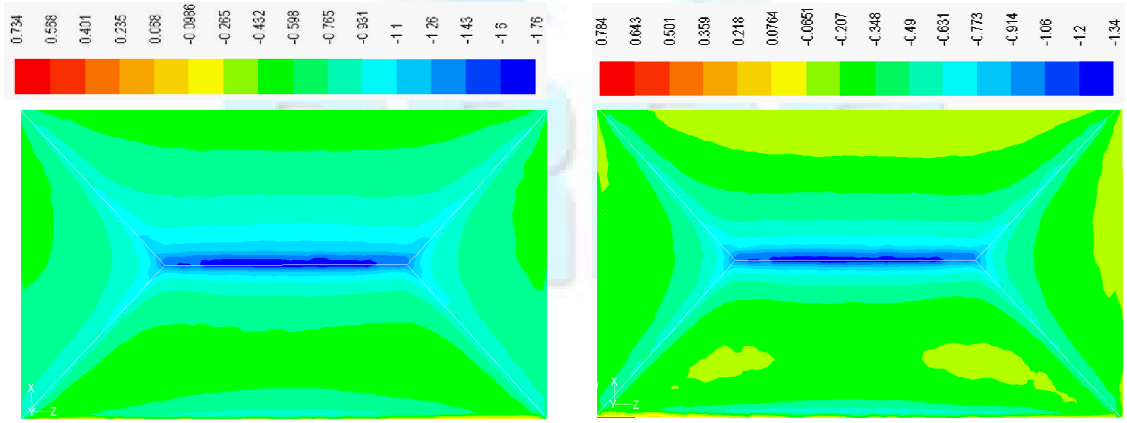

(a) P.C. on roof by Std. $k-\varepsilon$ turbulence model (b) P.C. on roof by RNG $k-\varepsilon$ turbulence model

Fig. 19 (a,b) Pressure Coefficients on the roof of the hip-roof building with 15 degree roof pitch at 0 degree wind attack angle

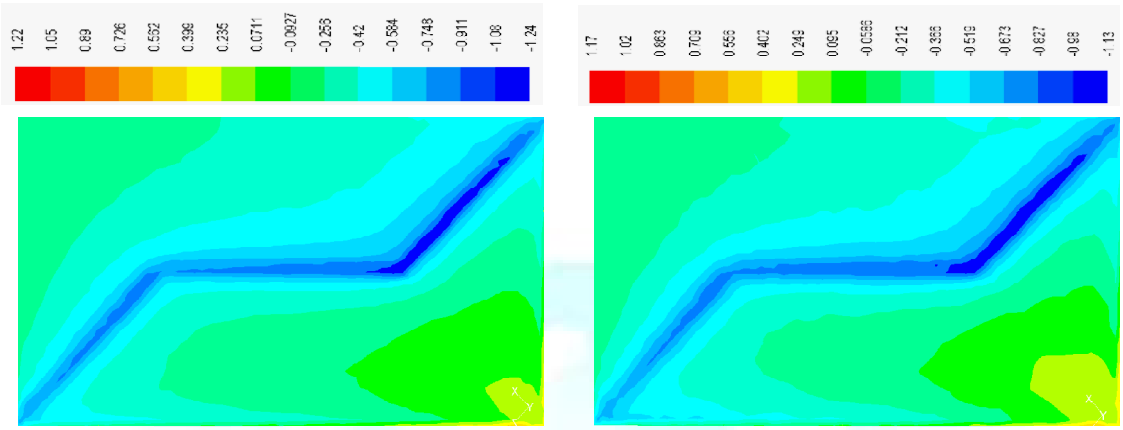

(a) P.C. on roof by Std. $k-\varepsilon$ turbulence model (b) P.C. on roof by RNG $k-\varepsilon$ turbulence model

Fig. 20 (a,b) Pressure Coefficients on the roof of the hip-roof building with 15 degree roof pitch at 45 degree wind attack angle

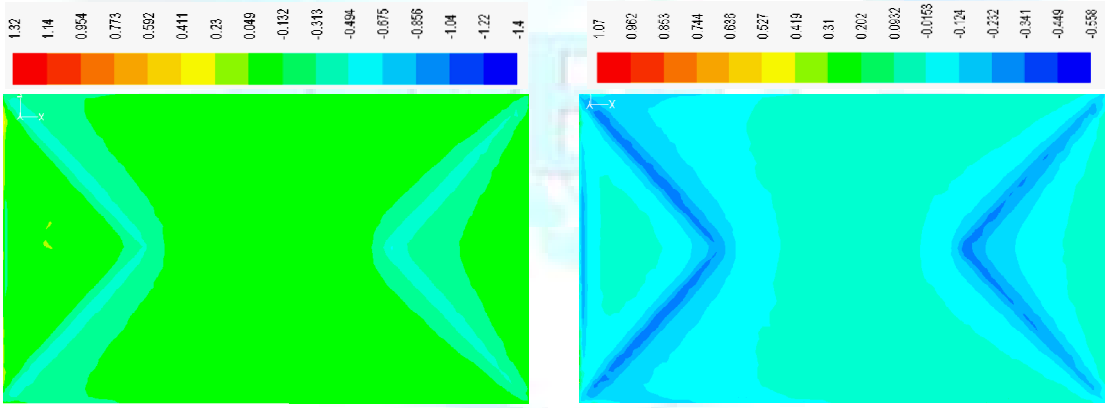

(a) P.C. on roof by Std. $k-\varepsilon$ turbulence model (b) P.C. on roof by RNG $k-\varepsilon$ turbulence model

Fig. 21 (a,b) Pressure Coefficients on the roof of the hip-roof building with 15 degree roof pitch at 90 degree wind attack angle

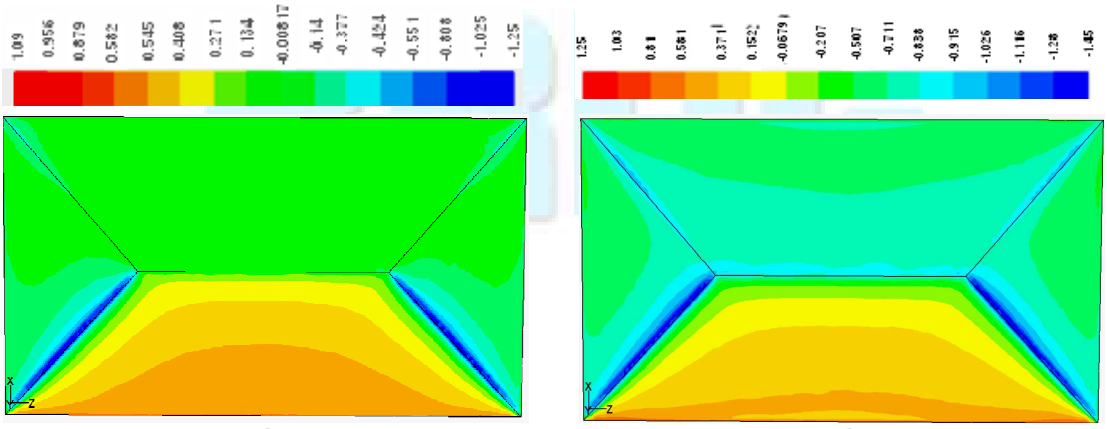

(a) P.C. on roof by Std. $k-\varepsilon$ turbulence model (b) P.C. on roof by RNG $k-\varepsilon$ turbulence model

Fig. 22 (a,b) Pressure Coefficients on the roof of the hip-roof building with 30 degree roof pitch at 0 degree wind attack angle

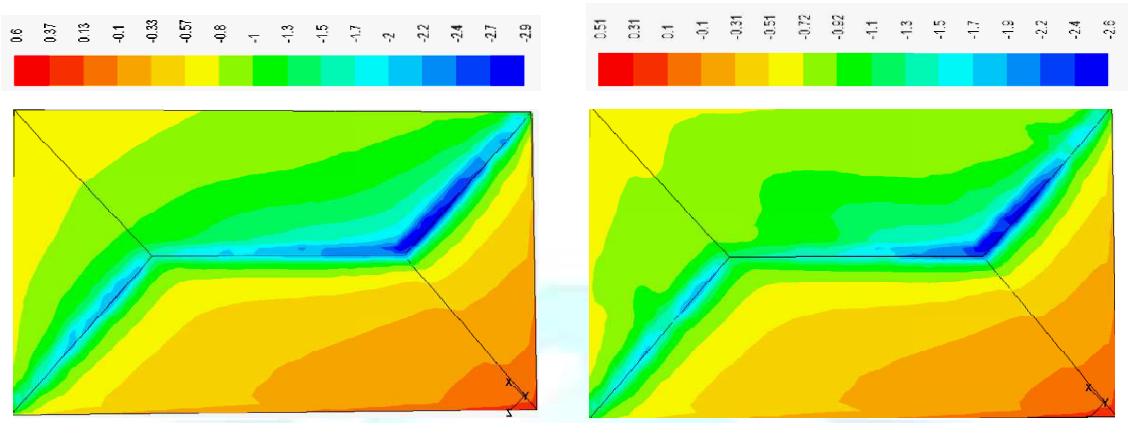

(a) P.C. on roof by Std. $k-\varepsilon$ turbulence model (b) P.C. on roof by RNG $k-\varepsilon$ turbulence model

Fig. 23 (a,b) Pressure Coefficients on the roof of the hip-roof building with 30 degree roof pitch at 45 degree wind attack angle

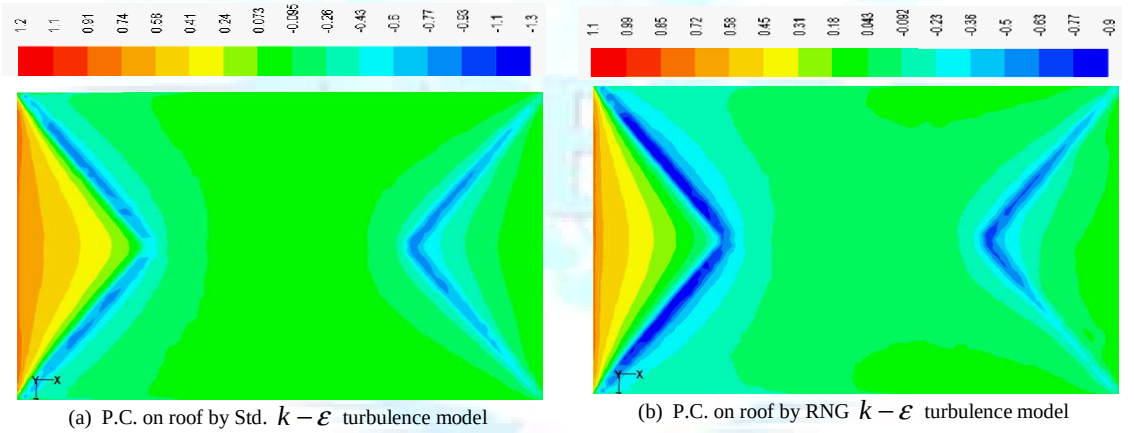

(a) P.C. on roof by Std. $k-\varepsilon$ turbulence model (b) P.C. on roof by RNG $k-\varepsilon$ turbulence model

Fig. 24 (a,b) Pressure Coefficients on the roof of the hip-roof building with 30 degree roof pitch at 90 degree wind attack angle

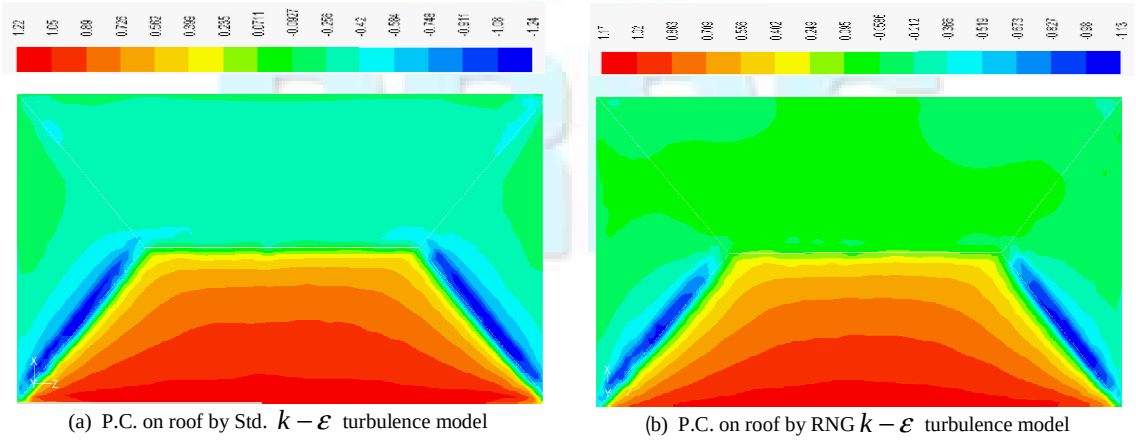

(a) P.C. on roof by Std. $k-\varepsilon$ turbulence model (b) P.C. on roof by RNG $k-\varepsilon$ turbulence model

Fig. 25 (a,b) Pressure Coefficients on the roof of the hip-roof building with 40 degree roof pitch at 0 degree wind attack angle

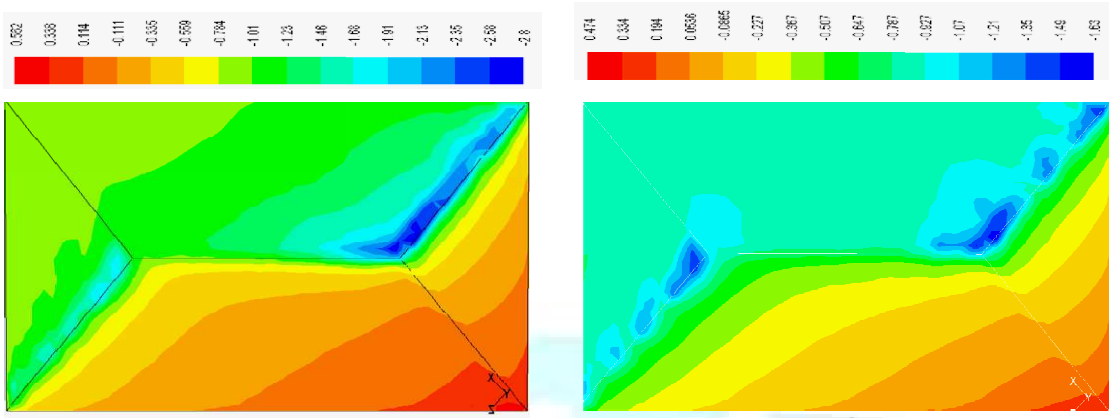

(a) P.C. on roof by Std. $k-\varepsilon$ turbulence model (b) P.C. on roof by RNG $k-\varepsilon$ turbulence model

Fig. 26 (a,b) Pressure Coefficients on the roof of the hip-roof building with 40 degree roof pitch at 45 degree wind attack angle

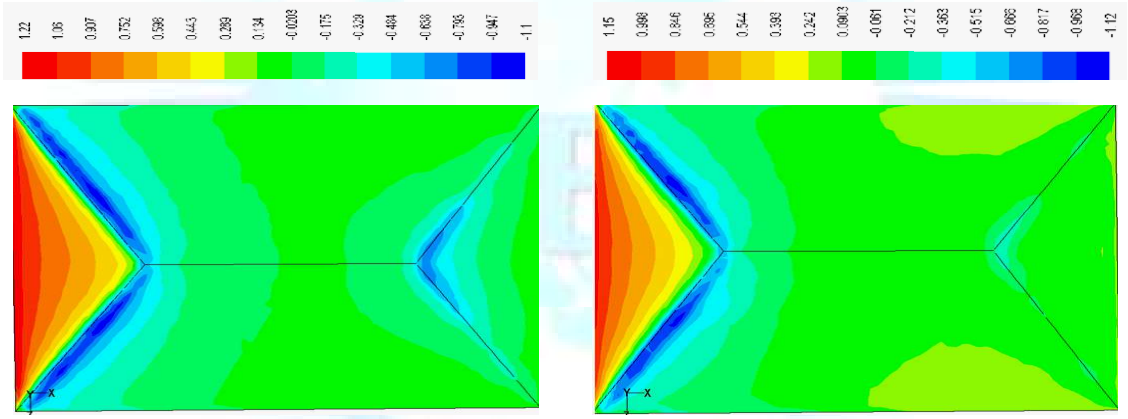

(a) P.C. on roof by Std. $k-\varepsilon$ turbulence model (b) P.C. on roof by RNG $k-\varepsilon$ turbulence model

Fig 27 (a,b) Pressure Coefficients on the roof of the hip-roof building with 40 degree roof pitch at 90 degree wind attack angle

SKE and RNGKE techniques, although values differ at some places. For zero degree incidence angle, the plot of both SKE and RNGKE technique shows that pressure coefficient values become more and more negative in the windward side as the roof pitch increases, while leeward side does not follows any trend as such. For 45 degree incidence angle, both SKE and RNGKE techniques show that maximum negative value of pressure coefficient occurred at ridge line in every case and its value decreases as the pitch increases. While for 90 degree roof wind incidence angle, the value of pressure coefficients remains almost zero throughout the curve for every case.

Fig. 19 to 27, gives the contour plots of pressure coefficients obtained using SKE and RNGKE techniques at different roof pitches. At zero wind incidence angle, for both the Standard $k-\varepsilon$ and the RNG $k-\varepsilon$ method the value of suction pressure coefficient decreases as roof pitch increases, with 40 degree roof pitch showing lowest value of suction pressure. Pressure coefficient distribution for the 45° wind incidence angle is very much different from that of the zero degree wind attack angle. The value of suction pressure increases with the increase in roof pitch but for 40 degree roof pitch it against falls to a lower negative value. Whereas at 90 degree roof pitch, the value of suction pressure increases with the value of roof pitch, with 15 degree having lowest suction pressure. Table 1 shows the maximum suction pressure coefficients at different roof pitches.

6. Conclusions

This project has witnessed the tests of two CFD simulation models; they are Standard $k-\varepsilon$ method and RNG $k-\varepsilon$ method. The values of the mean wind pressure coefficients

are compared with the available wind-tunnel data in order to check the accuracy of the CFD results.

And it can be concluded easily from the above findings that the numerical results fall in the range of the experimental data in general, but substantial discrepancies exists near the corners and sharp bends, and these discrepancies are because in the wind-tunnel experiments, the pressure coefficients were not recorded in the overhang portions and at the sharp bends. In these regions the pressure coefficients were either interpolated or extrapolated. Overall trend of the contours plotted for different wind attack angle as well as the numerical values remains approximately the same as that of the contour plot of Shakeel *et al* and Xu *et al*.

The results showed that the roof pitch significantly affects the roof pressure on the hip-roofs. Variation of roof-pitches has affected both magnitude as well as pattern of distribution. An increase in the pitch of a hip roof caused an increase in the (suction) pressure for all attack angles except for zero degree attack angle in which trend was reverse. While considering all cases, 30° hip roof, for 45° attack angle, experienced the maximum (suction) pressure at roof corner among the three tested hip roof models.

It has been found that the Standard $k-\varepsilon$ models have a good reputation for its efficiency and easy implementation. It has been recognized that the widely used Standard $k-\varepsilon$ model can predict the general wind conditions around the building reasonably well, except those in the separation regions above roof surface. This can be attributed to the overestimation of turbulence energy where the slope of the roof changes.

The RNG $k-\varepsilon$ turbulence model was found to be the best choice among the RANS models for rapid solutions. It gave encouraging results for the mean pressure coefficients in most cases.

Accurate modeling of the boundary conditions on the incident flows such as the velocity profile and turbulence intensity profile in the numerical simulations is of great importance for getting good agreement between the numerical results and experimental measurements.

Acknowledgement

The authors wish to thank Council of Science and Technology, U.P., India for providing grants for this project.

Abbreviations

CFD: Computational Fluid Dynamics
RANS: Reynolds Averaged Navier–Stokes Equations
SKE: Standard $k-\varepsilon$
RNG: Renormalization group (RNG) $k-\varepsilon$
MMK: Murakami, Mochida and Kondo
LK: Launder and Kato
LES: Large Eddy Simulation
DES: Direct Eddy Simulation
DNS: Direct Numerical Simulation

References

[1] Minimum design loads for building and other structures, American society of Civil Engineers, 2006.
[2] Building performance in hurricane Andrew in Florida observations, Recommendations and Technical Guidance, Federal Emergency Management Agency, Federal Insurance Administration, USA, 1992.
[1] A.G. Davenport, D. Surry, T. Stathopoulos, "Wind loads on low-rise buildings", final report of phase I and II, Boundary Layer Wind Tunnel Report BLWT-SS4, University of Western Ontario, Canada, 1978.
[2] P.R. Sparks, J. Baker, J. Belville, D.C. Perry, Hurricane Elena Gulf Coast August 29-Sept 2 Committee on Natural Disasters, Commission on Engineering and Technical Systems, Natural Research Council, U.S.A., 1985.
[3] D. Meecham, D. Surry, A.G. Davenport, "The magnitude and distribution of wind induced pressures on hip and gable roofs", Journal of Wind Engineering and Industrial Aerodynamics, Vol. 38, 1991, pp. 257–272,.
[4] Y.L. Xu, G.F. Reardon, "Variations of wind pressure on hip roofs with roof pitch", Journal of Wind Engineering and Industrial Aerodynamics, Vol. 73, 1998, pp. 267-284.
[5] S. Ahmad, K. Kumar, "Effect of Geometry on Wind Pressures on Low-rise Hip Roof Buildings", Journal of Wind Engineering and Industrial Aerodynamics, Vol. 90, 2002, pp. 755-779.
[6] The user guide of Fluent, Fluent. Inc. 6.2.3, 2006.
[7] S. Ghosal, P. Moin, "The basic equations for large eddy simulation of turbulent flows in complex geometries", Journal of Computational Physics, Vol. 118, 1995, pp. 24-37.
[8] S. Huang, Q.S. Li, S. Xu, "Numerical evaluation of wind effects on a tall steel building by CFD", Journal of Constructional Steel Research, Vol. 63, 2007, pp. 612-627.
[9] Q.S. Li, J.Q. Fang, A.P. Jeary, D.A. Paterson. "Computation of wind loading on buildings by CFD", Hong Kong Institution of Engineers, Transactions 5, 1998, pp. 51-57.
[10] S. Murakami, "Overview of turbulence models applied in CWE-1997", Journal of Wind Engineering and Industrial Aerodynamics, Vol. 74-76, 1998, pp. 1-24.

[11] A. Mochida, Y. Tominaga, S. Murakami, R. Yoshie, T. Ishihara, R. Ooka, "Comparison of various k-ε models and DSM to flow around a high rise building – report of AIJ cooperative project for CFD prediction of wind environment", Journal of Wind & Structures, Vol. 5, No. 2-4, 2004, pp. 227-244.

[12] N. G. Wright, G. J. Easom, "Non-linear k-ε turbulence model results for flow over a building at full scale", Applied Mathematical Modelling, Vol. 27, 2003, pp. 1013-1033.

[13] V. Yakhot, S.A. Orszag, S. Thangam, T.B. Gatski, C. G. Speziale, "Development of turbulence models for shear flows by a double expansion technique", Physics of Fluids, Vol. A4,1992, pp. 1510-1520.

[14] T.H. Shih, W. W. Liou, A. Shabbir, Z. Ynag, J. Zhu, "A new k-ε Eddy- Viscosity model for high Reynolds number turbulent flows – Model development and validation", Computers Fluids, Vol. 24, No. 3, 1995, pp. 227-238.

[15] J. Smagorinsky. "General circulation experiments with the primitive equations. I. the basic experiment", Monthly Weather Review, Vol. 91, 1963, pp. 99-164.

[16] W. Rodi, "Large eddy simulation of the flow past bluff bodies, Closure strategies for turbulent and transitional flows", Cambridge University Press, Cambridge, 2002, pp. 361-391.

[17] M. Germano, U. Piomelli, P. Moin, W.H. Cabot, "A dynamic subgrid scale eddy viscosity model", Physics of Fluids, Vol. A3, No. 7, 1991, pp. 1760-1765.

[18] D.K. Lily, "A proposed modification of the Germano subgrid-scale closure model", Physics of Fluids, Vol. 4 1992, pp. 633-635.

[19] F. Nicoud, F. Ducros, "Subgrid-scale stress modelling based on the square of the velocity gradient tensor", Flow, Turbulence and Combustion, Vol. 62, No. 3, 1999, pp. 183-200.

[20] W. W. Kim, S. Menon, "Application of the localized dynamic subgrid-scale model to turbulent wall-bounded flows", Technical report AIAA-97-0210. Reno (NV): American Institute of Aeronautics and Astronautics, 35thAerospace Science Meeting, 1997.

[21] K. Nozawa, T. Tamura, "Large eddy simulation of the flow around a low-rise building immersed in a rough-wall turbulent boundary layer", Journal of Wind Engineering and Industrial Aerodynamics, Vol. 90, 2002, pp. 1151-1162.

[22] Y. Ono, T. Tamura, H. Kataoka, "LES analysis of unsteady characteristics of conical vortex on a flat roof", in Proceedings of the 4th International 37 Symposium on Computational Wind Engineering (CWE 2006), Yokohama-Japan, 2006, pp. 373-376.

[23] H. C. Lim, T. G. Thomas, I. P. Castro, "Flow around a cube in a turbulent boundary layer: LES and experiment", Journal of Wind Engineering and Industrial Aerodynamics, Vol. 97, 2009, pp. 96-109.

[24] The user guide of Gambit, Gambit. Inc.2.6, 2006.

[25] S. Murakami, A. Mochida, Y. Hayashi, S. Sakamoto, "Numerical study on velocity pressure field and wind forces for bluff bodies by k−ε , ASM and LES", Journal of Wind Engineering and Industrial Aerodynamics, Vol. 41-44, 1992, pp. 2841-2852.